2018

Practical Method to Predict the Axial Capacity of RC Columns Exposed to Standard Fire

Salah El-Din F. El-Fitiany
The University of Western Ontario

Maged Youssef
youssef@uwo.ca

emerald PUBLISHING

Journal of Structural Fire Engineering

PRACTICAL METHOD TO PREDICT THE AXIAL CAPACITY OF RC COLUMNS EXPOSED TO STANDARD FIRE

Journal:	*Journal of Structural Fire Engineering*
Manuscript ID	JSFE-08-2016-0015.R1
Manuscript Type:	Research Paper
Keywords:	Column, Axial Capacity, Standard Fire, Average Temperature

PRACTICAL METHOD TO PREDICT THE AXIAL CAPACITY OF RC COLUMNS EXPOSED TO STANDARD FIRE

Abstract

Existing analytical methods for the evaluation of fire safety of Reinforced Concrete (RC) structures require extensive knowledge of heat transfer calculations and the finite element method. This paper proposes a rational method to predict the axial capacity of RC columns exposed to standard fire. The average temperature distribution along the section height is first predicted for a specific fire scenario. The corresponding distribution of the reduced concrete strength is then integrated to develop expressions to calculate the axial capacity of RC columns exposed to fire from four faces. These expressions provide structural engineers with a rational tool to satisfy the objective-based design clauses specified in the National Code of Canada in lieu of the traditional prescriptive methods.

Introduction

During fire events, elevated temperatures dramatically reduce the mechanical properties of concrete and steel. They also induce thermal and transient creep strains (Lie et al. 1992). To ensure that a fire exposed structure retains its integrity during the firefighting process; capacities of RC columns need to be monitored at different durations of fire exposure.

Current North America's building codes achieve the required fire ratings using prescriptive methods. These methods specify minimum cross-section dimensions and minimum clear cover to the reinforcing bars (CSA A23.3-04). Objective-Based Design (OBD) was first introduced in the 2005 National Building Code (NBCC 2005). Engineers are given the option to adhere to the specified acceptable solutions, prescriptive design, or develop innovative & economical solutions that achieve equivalent level of performance. This addition to the code is still not fully utilized in many aspects of structural design, including structural fire safety, due to the complex phenomena associated with structural behavior under fire exposure.

Capacity of RC columns during fire events can be evaluated using nonlinear coupled thermal-stress Finite Element (FE) analysis. Raut and Kodur (2011) concluded that the FE method is a powerful tool to predict the behavior of RC columns during fire exposure. Drawbacks of using the FE method, including: the need for a comprehensive computer program, the difficulty to comprehend its results and to identify potential modeling errors, and the long running time, make it impractical for design engineers. A simplified sectional analysis method to estimate the axial behavior of RC columns during fire exposure was proposed and validated by El-Fitiany and Youssef (2009, 2010, and 2011) and Law and Gillie (2010). The method involves dividing the cross-section into horizontal layers and converting the two-dimensional (2D) temperature distribution within the section to a rational average one-dimensional (1D) distribution. The average

temperature is used to predict the section tangent stiffness and the axial load-axial deformation relationship. Although sectional analysis is relatively easy to apply as compared to FE, it requires evaluating the temperature distribution within the concrete section based on knowledge of heat transfer principles. It also requires solving the equilibrium and kinematic equations utilizing different constitutive relationships for the section layers (Caldas et al. 2010).

Dotreppe et al. (1999) proposed a simple equation to predict the fire resistance of RC columns. This equation was based on a number of FE numerical simulations, and, thus is limited to the studied cases: standard fire exposure (ISO 834, ASTM-E119, and ULC-S101), columns with cross-sectional areas less than $0.2\ m^2$ and aspect ratios (h/b) greater than 0.5 (where h and b are the section's height and width, respectively).

In this paper, a simplified method to predict the axial capacity of RC columns exposed to fire is developed. It eliminates the need to divide a fire exposed section into elements or layers to conduct the heat transfer and stress analyses calculations. The proposed expressions are mathematically derived based on several rational assumptions and can be easily applied by practitioners to evaluate the average concrete temperature, the average concrete stress, the stress in the steel bars, and the column's reduced axial capacity. A similar approach suitable for columns subjected to combined flexure moments and axial forces was proposed by El-Fitiany and Youssef (2014). This paper discusses the axial behavior of RC columns, evaluates errors associated with some simplifying assumptions, and provides the derivation and validation of the proposed method.

Axial Behavior of RC Columns Exposed to Fire

Section Analysis Method

Fig. 1a shows a 305 mm square column, column $C1$ in Table 1, exposed to fire from its four sides and tested by Lie et al. (1984). The sectional analysis method developed and validated by El-Fitiany and Youssef (2009) is used to calculate the axial capacity of this column using the following steps:

1. At specific fire duration, the section is divided into a number of two dimensional elements, Fig. 1a, and the temperature distribution is predicted using the Finite Difference Method (FDM) (Lie et al. 1992). The effect of steel bars is neglected in the heat transfer analysis. Fig. 1b shows the predicted elevated temperatures after 1 hr of ASTM-E119 fire exposure.
2. The section is divided into horizontal layers and two average temperatures, T_σ and T_{avg}, are calculated for each layer, Fig. 2. T_σ results in the same average concrete compressive strength for the considered layer, and, thus is suitable for strength calculations. T_{avg} represents the algebraic average temperature of the elements within each layer and is suitable for thermal and transient creep strains calculations (Youssef and Moftah 2007).
3. The total concrete strain at elevated temperatures (ε) is composed of three terms (Youssef and Moftah 2007): unrestrained thermal strain (ε_{th}), instantaneous stress related strain (ε_c), and transient creep strain (ε_{tr}). The total strain is given by Eq. (1).

$$\varepsilon = \varepsilon_{th} + \varepsilon_c + \varepsilon_{tr} \quad (1)$$

The nonlinear thermal strain (ε_{th}) distribution, Fig. 3f, is calculated using T_{avg}. The thermal strain of steel bars is calculated based on the concrete temperature at their locations. ε_{th} is then converted to an equivalent linear thermal strain (ε_i), Fig. 3c, by considering self-equilibrium of internal thermal forces in concrete and steel layers. Fig. 3e shows the differences between the

equivalent linear and nonlinear thermal strains, which represent the self-induced thermal strains (ε_{st}). These strains are assigned as initial strains for the concrete and steel layers to model the corresponding self-induced self-equilibrating thermal stresses. The terms ε_{st}, ε_c, and ε_{tr} are lumped into an equivalent mechanical strain ε_{cT}, Eq. (2), which can be used in the constitutive stress-strain relationship for concrete developed by Youssef and Moftah (2007).

$$\varepsilon = \varepsilon_i + (\varepsilon_{st} + \varepsilon_c + \varepsilon_{tr}) = \varepsilon_i + \varepsilon_{cT} \quad (2)$$

4. For different values of ε_{cT}, the constitutive relationship by Youssef and Moftah (2007) is used to evaluate the internal stress for each layer. Considering equilibrium of the stresses for different layers, the corresponding axial force is calculated.
5. The previous steps are repeated at different fire temperatures. The axial load (P)–axial strain (ε) curves at $t = 0.0$, 1.0, and 3.0 hrs are shown in Fig. 4. The peak points of these diagrams define the axial capacities of the analyzed section at different fire durations.

Error Analysis

The errors resulting from ignoring ε_{st} or using T_{avg} for strength calculations are assessed by analyzing the columns shown in Table 1. Comparisons between the analytical axial capacities obtained by considering all parameters, ignoring ε_{st}, and using T_{avg} are shown in Figs. 5a and 5b. While ignoring ε_{st} leads to slight underestimation of the axial capacity, using T_σ for stress calculations has a minor effect on the axial capacity of the examined concrete columns.

Proposed Method

The proposed method is based on the fact that the temperature distribution is steep close to the heated faces and almost constant at the core of the column section, Fig. 1b. Consequently, the

concrete strength is variable near the heated faces and constant at the inner concrete core. Application of the proposed method involves the following steps:

1) Evaluating a one-dimensional average temperature distribution for a specific fire scenario.

2) Choosing a mathematical expression to represent the predicted average temperature distribution.

3) Estimating the concrete strains at failure.

4) Evaluating the corresponding concrete and steel stresses.

5) Determining the axial capacity of the section.

Assumptions and derivations of simplified equations to conduct each of the mentioned steps are given in the following sections.

Average Temperature Distribution

Any type of heat transfer analysis can be utilized to predict the average temperature distribution along the height of a fire exposed section. In this paper, a simplified method to calculate the elevated temperature distribution is first presented. The section is then divided into regions of constant and variable temperatures. Equations to evaluate the average temperature profile for the cross-section are derived.

Wickstrom Simplified Formulas

Wickstrom (1986) proposed and validated a set of handy formulas to calculate the temperature distribution within a fire exposed concrete section. Wickstrom's formulas can be applied for any type of concrete and fire scenario. However, they are practically easy for ISO 834 standard fire and normal weight concrete. Wickstorm's formulas do not account for variability in the thermal

conductivity of concrete, moisture content, and nonlinear boundary conditions which include prescribed temperature and heat flux (Wickstrom 1986).

Fig. 6 shows a RC concrete column subjected to fire from four sides; Left (L), Right (R), Bottom (B), and Top (T) faces. Application of Wickstrom's formulas to calculate the temperature distribution within this section can be summarized as follows:

1) The fire temperature T_f in Celsius is first calculated at a specific fire duration t (hr) using a prescribed fire temperature-time relationship.
2) An equivalent ISO 834 fire duration (t^*) is then calculated. t^* evaluates the corresponding time of exposure to the standard ISO 834 standard fire to result in a fire temperature T_f. The ratio between the modified time (t^*) and the actual fire duration (t) defines a dimensionless compartment time factor (Γ). The ISO 834 standard fire can be described by Eq. (3).

$$T_{f\,(\mathrm{ISO})} = 345\ \log(480\,t^* + 1) \tag{3}$$

where $T_{f\,(\mathrm{ISO})}$ is the ISO 834 standard fire temperature in Celsius at a modified fire duration t^* in hrs.

3) The temperature rise at any point (x, y) within the section due to heating from four sides can be estimated using Eq. (4).

$$T_{xy} = \left[n_w\left(n_x + n_y - 2n_x.n_y\right) + n_x.n_y\right] T_f \tag{4a}$$

$$n_w = 1 - 0.0616\left(\sqrt{\Gamma}.\ t\right)^{-0.88} \qquad \geq 0.0 \tag{4b}$$

$$n_x = \left[0.18\ln\left(\frac{t}{x^2}\right) - 0.81\right]_{\text{Fire (L)}} + \left[0.18\ \ln\left(\frac{t}{(b-x)^2}\right) - 0.81\right]_{\text{Fire (R)}} \qquad \geq 0.0 \tag{4c}$$

$$n_y = \left[0.18\ln\left(\frac{t}{y^2}\right) - 0.81\right]_{\text{Fire (T)}} + \left[0.18\ \ln\left(\frac{t}{(h-y)^2}\right) - 0.81\right]_{\text{Fire (B)}} \qquad \geq 0.0 \tag{4d}$$

where b is the section width, h is the section height, T_{xy} is the temperature rise at any point (x, y) in Celsius, n_w is the ratio between the surface temperature and the fire temperature, and n_x and

n_y are the ratios between the internal and surface temperatures due to heating in the x and y directions, respectively.

Temperature Regions

Figs. 6 and 7 show different temperature regions within a concrete section. The values shown in each region indicate the heating surface causing temperature variation in x and y directions. Values of zero indicate that the temperature is constant in the given direction. While region R2(0,0), Fig. 6, is not affected by the fire temperature, region R3(L+R, T+B), Fig.7, is affected by fire temperature from the four sides. The value of z that defines the boundaries of these regions can be evaluated by equating n_x and n_y in Eqs. (4c) and (4d) to zero, which will result in Eq. (5). Value of z is less than $b/2$ and $h/2$ in Fig. 6 and are greater than them in Fig. 7.

$$z = \sqrt{e^{-4.5}\ t} \tag{5}$$

The schematic temperature profiles for lines 1-1 and 2-2 in Fig. 6 present the variation of temperature in x direction at $y \leq z$ and $y = z \rightarrow (h - z)$, respectively. Both profiles show varying temperature for R1 and constant temperature for R2. The schematic temperature profiles for lines 1-1 and 2-2 in Fig. 7 present the variation of temperature in the x direction at $y \leq (h - z)$ and $y = (h - z) \rightarrow z$, respectively. All regions have variable temperature profile.

Average Temperatures

Eq. (4a) predicts the temperature rise at different locations within the studied concrete section. For each of lines 1-1 and 2-2, n_y is constant and n_x value defines the temperature along the line. To conduct uniaxial stress analysis for the fire exposed section, the average temperature for each line needs to be calculated. Three equations are derived to evaluate the average temperature within

each region at a given y value. $T_{avg\,1}$, Eq. (6a), represents the average temperature for regions affected by heating from either L or R. $T_{avg\,2}$, Eq. (6b), represents the average temperature for regions not affected by heating from L or R. $T_{avg\,3}$, Eq. (6c), represents the average temperature due to heating from the left and right sides simultaneously, i.e. (L + R).

$$T_{avg\,1} = \left[0.18\,n_w - 0.36\,n_w.n_y + 0.18\,n_y\right]\left[x_2\ ln\left(\frac{t}{{x_2}^2}\right) - x_1\,ln\left(\frac{t}{{x_1}^2}\right)\right]\frac{T_f}{(x_2-x_1)}$$

$$-0.45\,T_f.n_w + 1.9\,T_f.n_w.n_y - 0.45\,T_f.n_y \qquad x = x_1 \rightarrow x_2 \qquad (6a)$$

$$T_{avg\,2} = T_f.n_w.n_y \qquad (6b)$$

$$T_{avg\,3} = \left(0.18\,n_w + 0.18\,n_y - 0.36\,n_w.n_y\right)\left[ln\left(\frac{t}{(b-x_2)^2}\right)\,x_2 - ln\left(\frac{t}{(b-x_1)^2}\right)\,x_1\right]\frac{T_f}{(x_2-x_1)}$$

$$+\,b\left(0.36\,n_w.n_y - 0.18\,n_w - 0.18\,n_y\right)\left[ln\left(\frac{t}{(b-x_2)^2}\right) - ln\left(\frac{t}{(b-x_1)^2}\right)\right]\ \frac{T_f}{(x_2-x_1)}$$

$$-0.45\,T_f.n_w + 0.9\,T_f.n_w.n_y - 0.45\,T_f.n_y + T_{avg\,1} \qquad x = x_1 \rightarrow x_2 \qquad (6c)$$

The average temperatures $T_{avg\,1}$, $T_{avg\,2}$, and $T_{avg\,3}$ are represented in Figs. 6 and 7 by the dashed lines. The ambient temperature (20 °C) is added to the calculated average temperatures. A weighted average temperature can then be calculated for each line to facilitate sketching the final average temperature distribution along the section height. The final temperature profile can be idealized using Eq. (7) where z_1 and z_2 are constants that can be estimated using average temperature values at $y = 0.0$ and $y = z$. This equation was chosen as it can be easily integrated.

$$T_{avg} = z_1\,.\,e^{(z_2\,.\,y)} \qquad (7)$$

where $z_1 = T_{avg\,(y=0.0)}$; and $z_2 = \frac{\ln\left[\frac{T_{avg\,(y=z)}}{z_1}\right]}{z}$

Concrete Fire-induced Strains

The total concrete strain at elevated temperatures (ε) is given by Eq. (2) (Youssef and Moftah 2007, Terro 1998). The thermal deformations shift the axial load (P)–axial strain (ε) diagrams but do not affect the axial capacity of the studied section, Fig. 4. This fact allows ignoring ε_i in the proposed method as it will not affect the member capacity. The effect of self-induced strains (ε_{st}) on the axial capacity is found to have minor effect on the predicted member capacity, Fig. 5a.

The value of ε_c at the peak stress (f'_{cT}), i.e. ε_{oT}, defines the stress-strain relationship during fire exposure. For loaded RC columns, the effect of elevated temperatures on ε_{oT} is negligible (Youssef and Moftah 2007). Fig. 8 shows the variation of $\varepsilon_{oT} + \varepsilon_{tr}$ with fire temperature (Eurocode 2-1992). A linear relationship, i.e. Eq. (8), is chosen to represent the Eurocode 2 recommendation. Such a relationship allows reaching a closed form solution while accounting for concrete nonlinearity as will be discussed in the next section. To evaluate the error associated with using the approximate Eq. (8), the axial capacities of the columns shown in Table 1 are calculated up to 4 hrs of ASTM-E119 standard fire exposure. Fig. 9a shows that this approximation has a negligible effect on the axial capacity predictions calculated using sectional analysis method.

$$\varepsilon_{oT} + \varepsilon_{tr} = 2.52\times10^{-5}\, T_{avg} \qquad 80\ ℃ < T_{avg} \leq 1200\ ℃ \qquad (8)$$

Concrete subjected to lower T_{avg} develops their compressive capacity at lower ε_{cT}. Thus, failure strain is defined using the lowest T_{avg} in the section.

Stress-Strain Relationships

Concrete

Concrete compressive strength experiences significant degradation at elevated temperatures. Eurocode 2 predicts the reduced compressive strength (f'_{cT}) for siliceous and carbonate concretes

as a ratio from its ambient value (f'_c) (Eurocode 2-1992). The reduction in f'_{cT} for siliceous concrete is fitted by a polynomial equation, Eq. (9). For $T_{avg} \leq 900$ ℃, the proposed equation results in coefficient of variations of 0.067 and 0.195 for siliceous and carbonate concrete, respectively. Fig. 9b shows the axial load capacities of the columns in Table 1 considering either siliceous or carbonate concrete. Carbonate aggregate slightly increases the axial capacity of RC columns during fire exposure, and, thus the use of Eq. (9) yields conservative predictions.

$$f'_{cT}/f'_c = 1.76\times10^{-9}\,T_{avg}{}^3 - 3.00\times10^{-6}\,T_{avg}{}^2 + 2.50\times10^{-4}\,T_{avg} + 1.00 \quad (9)$$

where T_{avg} is the weighted average temperature, in ℃, calculated in previous section

The relationship between the compressive stress, f_{cT}, and the corresponding mechanical strain, ε_{cT}, at elevated temperatures was studied by a number of researchers. Among the available models, Youssef and Moftah (2007) proposed a stress-strain model, Eq. (10), which includes a simplified representation of transient creep strains and better matches the available experimental data. It is also consistent with the Eurocode 2 stress-strain relationship. Fig. 10 shows the concrete stress-strain relationship at three average temperatures ($T_{avg} = 230$, 400, and 600 ℃). f'_{cT} and $\varepsilon_{oT} + \varepsilon_{tr}$ are calculated using Eqs. (8) and (9), respectively.

$$f_{cT} = f'_{cT}\left[2\left(\frac{\varepsilon_{cT}}{\varepsilon_{oT}+\varepsilon_{tr}}\right) - \left(\frac{\varepsilon_{cT}}{\varepsilon_{oT}+\varepsilon_{tr}}\right)^2\right] \qquad \varepsilon_{cT} \leq (\varepsilon_{oT} + \varepsilon_{tr}) \quad (10)$$

The axial behavior of RC columns during fire exposure can be predicted by assuming different mechanical strains (ε_{cT}). At each ε_{cT}, the corresponding concrete stresses at different y values are calculated using Eqs. (9) and (10). The axial load is then predicted by summing the normal concrete stresses.

Using the average temperature distribution defined by Eq (7), the distribution of $\varepsilon_{oT} + \varepsilon_{tr}$ and f'_{cT}/f'_{c} over the section height can be evaluated using Eqs. (8) and (9). The minimum value of $\varepsilon_{oT} + \varepsilon_{tr}$ defines the failure strain ε_{cT}. The distribution of stresses over the section height can then be evaluated using Eq. (10). Integrating these stresses over a distance y of the section height results in an average concrete stress, Eq. (11).

$$\left(\frac{f_{cT\,avg}}{f'_c}\right) = 2\left(\frac{f_{cT\,avg}}{f'_c}\right)_L - \left(\frac{f_{cT\,avg}}{f'_c}\right)_N \tag{11}$$

where

$$\left(\frac{f_{cT\,avg}}{f'_c}\right)_L = \left(\frac{6.566\times10^{-6}\,\varepsilon_{cT}}{z\,z_1\,z_2}\right)\left[5.3\,z_1{}^3\,e^{2\,z\,z_2} - 1.815\times10^4\,z_1{}^2\,e^{z\,z_2} - 6.055\times10^9\,e^{-z\,z_2}\right.$$

$$\left. +1.516\times10^6\,z\,z_2\,z_1 - 5.3\,z_1{}^3 + 1.815\times10^4\,z_1{}^2 + 6.055\times10^9\right] \quad \text{, and}$$

$$\left(\frac{f_{cT\,avg}}{f'_c}\right)_N = \left(\frac{52\times10^{-2}\,\varepsilon_{cT}{}^2}{z\,z_1{}^2\,z_2}\right) * \left[5.3\,z_1{}^3\,e^{z\,z_2} - 1.514\times10^9\,e^{-2\,z\,z_2} - 7.58\times10^5\,z_1\,e^{-z\,z_2}\right.$$

$$\left. -9.077\times10^3\,z\,z_2\,z_1{}^2 - 5.3\,z_1{}^3 + 7.58\times10^5\,z_1 + 1.514\times10^9\right]$$

Steel

Lie et al.'s model (1992) is used to predict the reduced yield strength of reinforcing bars (f_{yT}), Eq. (12), and the stress-strain ($f_{sT} - \varepsilon_{sT}$) relationship, Eq. (13).

$$f_{yT} = \left[1 + \frac{T}{900\,\ln(T/1750)}\right] f_y \qquad 0 < T \le 600\ ^\circ\text{C} \tag{12a}$$

$$= \left[\frac{340 - 0.34\,T}{T - 240}\right] f_y \qquad 600 < T \le 1000\ ^\circ\text{C} \tag{12b}$$

$$f_{sT} = \frac{f[T\,,0.001]}{0.001}\,\varepsilon_{sT} \qquad \varepsilon_{sT} \le \varepsilon_p \tag{13a}$$

$$f_{sT} = \frac{f[T\,,0.001]}{0.001}\,\varepsilon_p + f\left[T\,,\left(\varepsilon_{sT} - \varepsilon_p + 0.001\right)\right] - f[T\,,0.001] \qquad \varepsilon_{sT} > \varepsilon_p \tag{13b}$$

$$\varepsilon_p = 4\times10^{-6}\,f_y \tag{13c}$$

$$f[T, 0.001] = (50 - 0.04\,T)\left[1 - e^{(-30+0.03\,T)\sqrt{0.001}}\right]\times 6.9 \quad (13d)$$

$$f\left[T, (\varepsilon_{sT} - \varepsilon_p + 0.001)\right] = (50 - 0.04\,T)\left[1 - e^{(-30+0.03\,T)\sqrt{(\varepsilon_{sT}-\varepsilon_p+0.001)}}\right]\times 6.9 \quad (13e)$$

Predicting the Axial Capacity

The axial compression capacity is finally calculated by summing the forces in concrete and steel. The following section provides example calculations for the proposed method.

Illustrative Example

The column tested by Lie et al. (1984), Fig. 1, is used as an example to explain the proposed method. It has a section of 305 mm by 305 mm. It is reinforced with four 25 mm steel bars and has 10 mm ties spaced at 305 mm. The compressive and yield strengths of the siliceous concrete and reinforcing steel bars are 36.1 and 443.7 MPa, respectively. The column is exposed to a standard ASTM-E119 fire while being axially loaded. The calculated ambient axial compressive capacity of the column is 4120 kN. The following steps are conducted to calculate the axial capacity of the tested column after 1 hr and 3 hrs of ASTM-E119 fire exposure.

1) The ASTM-E119 fire temperature (T_f) is first calculated at fire durations of $t = 1.0\ hr$ and 3.0 hrs using Eq. (14), Lie et al. (1992).

$$T_f = 750\left(1 - e^{-3.79553\sqrt{t}}\right) + 170.41\sqrt{t} \quad (14)$$

where T_f is the fire temperature in Celsius and t (hrs) is the fire duration.

For t of 1 hr and 3 hrs, values of T_f are 904 ℃ and 1044 ℃, respectively.

2) Γ values of 0.86 and 0.74 for t of 1.0 hr and 3.0 hrs, respectively, are evaluated using Eq. (3).

3) n_w values of 0.93 and 0.97 for t of 1.0 hr and 3.0 hrs, respectively, are estimated using Eq. (4b).

4) z values of 0.105 m and 0.183 m for t of 1.0 hr and 3.0 hrs are calculated using Eq. (5).

5) The average temperatures for each region are calculated and are shown in Figs. 6 and 7 by the dashed lines.

For 1 hr fire exposure (Fig. 6): z of 0.105 is used to define the region boundaries. Substituting in Eq. (6a) using $x_1 = 0.0\,m$, and $x_2 = 0.105\,m$ results in $T_{avg\,1} = 304 + 562\,n_y$. Substituting in Eq. (6b) using $x_1 = 0.0\,m$, and $x_2 = 0.105\,m$ results in $T_{avg\,2} = 844\,n_y$.

For 3 hrs fire exposure (Fig. 7): z of 0.183 m is greater than $b/2$, thus the region boundary is defined by the value of ($b - 0.183\,m = 0.122\,m$). Using Eq. (6a), $x_1 = 0.0\,m$, and $x_2 = 0.122\,m$ results in $T_{avg\,1} = 512 + 518\,n_y$. Substituting in Eq. (6c) using x_1 of 0.122 m, and x_2 of 0.183 m results in $T_{avg\,3} = 136 + 884\,n_y$.

6) The ambient temperature (20 ℃) is added to the calculated average temperatures. Weighted average temperatures for t of 1.0 hr and 3.0 hrs are then calculated at different y values. For 1 hr fire exposure, $T_{avg}(y = 0.0\,m) = 879$ ℃ and $T_{avg}(y = 0.105\,m) = 230$ ℃. For 3 hrs of fire exposure, $T_{avg}(y = 0.0\,m) = 1048$ ℃ and $T_{avg}(y = 0.153\,m) = 534$ ℃. The average temperature distribution is shown in Fig. 11. The figure shows that the values calculated using the developed simplified method matches the values predicted using the FDM method.

7) The constants (z_1 and z_2) of Eq. (7) are evaluated using values of T_{avg} at y_1 of 0.0 m and y_2 of 0.105 m for t of 1 hr and at y_1 of 0.0 m and y_2 of 0.153 m for t of 3 hrs. The equations representing the average temperature distribution over the section height are:

For 1 hr of exposure, $T_{avg} = 879\ e^{(-12.12\ y)}$

For 3 hrs of exposure, $T_{avg} = 1048\ e^{(-4.41\ y)}$

8) The lowest average temperatures in the section for $t = 1\ hr$ and $t = 3\ hrs$ are 230 ℃ and 534 ℃, respectively. The failure strain ε_{cT} can be assumed to be equal to $\varepsilon_{oT} + \varepsilon_{tr}$. For t of 1 hr and 3 hrs, ε_{cT} equals to 5.80×10^{-3} and 13.47×10^{-3}, respectively.

9) Fig. 12 shows the constant strain distribution. The corresponding f_{cT} distributions for t of 1 hr and 3 hrs are also shown. Values of f_{cT} are evaluated using Eq. (10). $f_{cT\ avg}$ is calculated as follows:

   a. For t of 1 hr: substituting in Eq. (11) using $y = 0.105\ m$, $z_1 = 879$, $z_2 = -12.12$, and $\varepsilon_{cT} = 5.80\times10^{-3}$ yields $\left(f_{cT\ avg}/f'_c\right)_L = 0.358$, $\left(f_{cT\ avg}/f'_c\right)_N = 0.236$, and $\left(f_{cT\ avg}/f'_c\right) = 0.481$. $\left(f_{cT\ avg}/f'_c\right)$ for the constant temperature zone is calculated directly using Eq. (9) as 0.920.

   b. For t of 3 hrs: substituting in Eq. (11) using $y = 0.153\ m$, $z_1 = 1048$, $z_2 = -4.41$, and $\varepsilon_{cT} = 13.47\times10^{-3}$ yields $\left(f_{cT\ avg}/f'_c\right)_L = 0.204$, $\left(f_{cT\ avg}/f'_c\right)_N = 0.171$, and $\left(f_{cT\ avg}/f'_c\right) = 0.237$.

10) The temperature of steel bars can be calculated using the Wickstrom method (1986), Eq. (4a). In this example, all bars have the same temperature that can be calculated as follows:

   a. For 1 hr of fire exposure: using Eqs. (4c) and (4d), n_x and n_y are equal to 0.2. Eq. (4a) yields $T_{avg} = 322$ ℃.

   b. For 3 hrs of fire exposure, n_x and n_y are equal to 0.39. Eq. (4a) yields $T_{avg} = 668$ ℃.

11) The steel stress is calculated using Eqs. (12) and (13). For 1 hr of fire exposure, $f_{yT} = 0.79\ f_y$. $\varepsilon_{sT} = 5.80\times10^{-3}$, $\varepsilon_p = 0.0018$, $f[T, 0.001] = 122\ MPa$, $f\left[T, \left(\varepsilon_{sT} - \varepsilon_p + 0.001\right)\right] = 196\ MPa$, and $f_{sT} = 290\ MPa$. For 3 hrs of fire exposure, $f_{yT} = 0.26\ f_y$. $\varepsilon_{sT} = 12.47\times10^{-3}$,

$\varepsilon_p = 0.0018$, $f[T, 0.001] = 108\,MPa$, $f\left[T, \left(\varepsilon_{sT} - \varepsilon_p + 0.001\right)\right] = 108\,MPa$, and $f_{sT} = 142\,MPa$.

12) Using the steel and concrete stresses, the axial capacity of the example column is predicted as $2{,}618\,kN$ and $1{,}077\,kN$ after $1\,hr$ and $3\,hrs$ fire exposure, respectively.

The steps mentioned above are repeated for the studied RC column at different fire durations. The reduced axial capacity is estimated at each fire duration up to $3.75\,hrs$, Fig. 13. Although the proposed method results in conservative predictions, i.e. around 15% less than test results, it was able to match the profile of degradation of the axial capacity and provided values with good accuracy for design engineers. The proposed method can be applied to have a quick idea about the structural fire safety of RC columns.

Validation

The proposed method is used to predict the axial compression capacity of three concentrically loaded RC columns tested by Lie and Wollerton (1998); Dotreppe et al. (1997); and Hass (1986).

Lie and Wollerton (1998)

Table 2 shows the geometric and reinforcement properties of eighteen RC columns tested by Lie and Wollerton (1998). All columns were axially loaded with a load P_{app} and subjected to a standard ASTM-E119 fire. Values for P_{app} were kept constant during testing of all columns. The fire endurance time (t) was recorded at the end of each column test. The reinforcing steel cover was $48\,mm$ for all columns except column NO. 16, where it was $64\,mm$. Fig. 14a shows a comparison between P_{app}, the predicted axial capacity using the method proposed in this paper and

the method proposed by Dotreppe et al. (1999) and applied by Tan and Tang (2004). The method proposed in this paper provided good accuracy given the complexity of the problem.

Dotreppe et al. (1997)

Table 3 shows the properties of eight RC columns tested by Dotreppe et al. (1997). The columns were loaded by the shown loads, P_{app}. The heights of columns 1 to 3 and columns 4 to 8 were $3.90\,m$ and $2.10\,m$, respectively. All columns were exposed to a standard ISO 834 fire exposure and the fire endurance (t) for each column was recorded. The reinforcing steel cover was $25\,mm$ for all columns and the end conditions were pinned-pinned. Although all the loads were concentrically applied at the beginning of the fire test, the columns were affected by buckling. Dotreppe et al. (1999) proposed reducing the axial capacity by a buckling factor $\chi(\lambda)$, Eq. (15).

$$\chi(\lambda) = 1 - \frac{\lambda}{100} \qquad \lambda \leq 20 \tag{15a}$$

$$\chi(\lambda) = 0.80\left[\frac{20}{\lambda}\right]^{0.7\left(\frac{225-c}{200}\right)^5} \qquad 20 < \lambda \leq 70 \tag{15b}$$

$$\chi(\lambda) = 0.80\left[\frac{20}{\lambda}\right]^{0.7\left(\frac{\lambda}{70}\right)\left(\frac{225-c}{200}\right)^5} \qquad 70 < \lambda \tag{15c}$$

where λ is the column slenderness ratio and c is the concrete cover in mm.

The predicted axial capacities by the proposed method are reduced by the factor $\chi(\lambda)$. Fig. 14b shows a comparison between applied concentric loads (P_{app}) and the reduced axial capacity predictions. The estimated axial capacities are in good agreement with the applied loads. Dotreppe et al.'s method results in slightly better accuracy than the proposed method as shown in Fig. 14b. This can be due to the fact that this method was calibrated using these experimental results.

Hass (1986)

Table 4 shows properties of seven RC columns tested by Hass (1986). All the columns were subjected to a standard ISO 834 fire exposure. The reinforcing steel cover was $38\ mm$ and the end conditions were pinned-pinned. The predicted axial capacities by the proposed method are reduced by Dotreppe et al.'s buckling factor $\chi(\lambda)$ to account for buckling (Dotreppe et al. 1999). Fig. 14c shows a comparison between applied concentric loads (P_{app}) and the predictions of the proposed method. As shown in the figure, the proposed method underestimates the axial capacity of the tested RC columns. A similar scatter in the results was found by Tan and Tang (2004) using Dotreppe et al.'s method (1999). It should be noted that columns No. 1 and 2 have the same geometric, material, and loading conditions but their fire endurance differs by 64%.

Limitations of the Proposed Method

Although the proposed method is simple and practical, it has the following limitations.

1) It does not account for concrete spalling. This assumption is only valid for normal strength concrete (El-Fitiany and Youssef 2009). However, the spalling effect may be investigated by reducing the dimensions of the fire-exposed cross-section. The new reinforcement cover shall also be used, when predicating the elevated temperature of the reinforcing bars.
2) It adopts a simple representation for the transient strains. This representation is applicable for heating rates between 2 and 50 K/min (Eurocode 2-1992). For heating rates outside this range, the reliability of using the proposed method should be investigated.
3) It does not account for effect of buckling.

Summary and Conclusion

This paper provides structural engineers with a rational tool to predict the axial compression capacity of four-faces heated RC columns during fire events. The proposed tool can be applied using a simple spreadsheet. The proposed method starts by dividing the analyzed section into different temperature zones. Equations to evaluate the average temperature with each zone are developed. The average temperature distribution is then used to estimate the failure strain. Equations to evaluate the corresponding average concrete stress were developed by integrating the concrete stresses along the height of the cross section. The failure strain is used to evaluate the reinforcing bar stresses. The axial compressive capacity is then calculated by using the concrete average stress and the reinforcing bar stresses. The errors resulting from different approximations considered in this paper were found to be acceptable when evaluating the column axial capacity. The proposed method is validated by comparing its predictions with the test results of thirty-three RC columns. A good agreement is found between the proposed method and the experimental results. The presented work should be further validated for parametric and natural fires.

Acknowledgments

This research was funded by the Natural Sciences and Engineering Research Council of Canada (NSERC).

References

Caldas RB, Sousa J, João BM and Fakurya RH (2010) Interaction diagrams for reinforced concrete sections subjected to fire. Eng. Struct., 32(9), 2832–2838.

Cement Association of Canada (2006) Concrete design handbook, CAN/CSA A23.3-04. 3rd Ed., Ottawa, ON, Canada.

Dotreppe, JC, Franssen, JM and Vanderzeypen Y (1999) Calculation method for design of reinforced concrete columns under fire conditions. ACI Struct. J., 96(1), 9-18.

Dotreppe JC, Franssen JM, Bruls A, Baus R, Vandevelde P, Minne R, Nieuwenburg DV and Lambotte H (1997) Experimental research on the determination of the main parameters affecting the behaviour of reinforced concrete columns under fire conditions. Mag. Concrete Res., 49(179), 117-127.

El-Fitiany SF and Youssef MA (2014) Simplified Interaction Diagrams for Fire-Exposed RC Columns, Eng. Struct., vol 70, pp. 246-259.

El-Fitiany SF and Youssef MA (2010) A Simplified Sectional Analysis Approach for RC Elements during Fire Events. 6th International Conference on Structures in Fire, Michigan State University, East Lansing, MI, 239-246.

El-Fitiany SF and Youssef MA (2009) Assessing the flexural and axial behaviour of reinforced concrete members at elevated temperatures using sectional analysis., FSJ, 44(5), 691-703.

El-Fitiany SF and Youssef MA (2011) Stress Block Parameters for Reinforced Concrete Beams During Fire Events. Innovations in Fire Design of Concrete Structures, ACI SP-279, 1-39.

Eurocode 2 (1992) Design of Concrete Structures. ENV EC2, Brussels.

Hass R (1986) Practical rules for the design of reinforced concrete and composite columns submitted to fire. Technical Rep. No. 69, Institute fur Baustoffe, Massivbau and Brandschutz der Technischen Universita Branschweig. (in German)

Law, A., and Gillie, M. (2010) Interaction Diagrams for Ambient and Heated Concrete Sections, Eng. Struct., 32(6), pp. 1641-1649.

Lie TT, and Woollerton J L (1998) Fire resistance of reinforced-concrete columns: Test results. Internal Rep. No. 569, National Research Council of Canada, Quebec, Canada.

Lie TT (1992) Structural fire protection. ASCE Manuals and Reports on Engineering Practice, no. 78, New York, 241 pp.

Lie TT, Lin TD, Allen DE, Abrams, MS (1984) Fire resistance of reinforced concrete columns. Technical Paper No. 378, Division of Building Research, National Research Council of Canada, Ottawa, Ontario, Canada.

NBCC (2005) National Building Code of Canada. National Research Council, Ottawa, ON.

Raut N and Kodur VKR (2011) Modeling the fire response of reinforced concrete columns under biaxial bending. ACI Struct. J., 108(6), 1-24.

Tan KH, Tang CY (2004) Interaction Formula for Reinforced Concrete Columns in Fire Conditions. ACI Struct. J., 101(1), 19-28.

Terro MJ (1998) Numerical modeling of the behavior of concrete structures in fire. ACI Struct. J., 95(2), 183-193.

Wickstrom U (1986) A very simple method for estimating temperature in fire exposed concrete structures. Fire Technology Technical report SP-RAPP 1986, 46, Swedish National Testing Institute, 186-194.

Youssef MA and Moftah, M (2007) General stress-strain relationship for concrete at elevated temperatures. Eng. Struct., 29(10), 2618-2634.

Tables and Figures

Table 1–Parametric study cases

Col #	b (mm)	h (mm)	f'_c (MPa)	f_y (MPa)	ρ $\%\ (A_g)$
$C1$	305	305	36.1	443.7	2.1
$C2$	400	400	30	400	1.5
$C3$	600	600	40	400	1.5
$C4$	400	700	50	400	1.0
$C5$	500	700	25	400	1.0

* all columns are analyzed up to 4 hrs of standard ASTM-E119 fire exposure

Table 2–Details of Lie and Wollerton (1998)

No	b (mm)	h (mm)	steel bars (mm)	f'_c (MPa)	f_y (MPa)	P_{app} (kN)	t (min)
1	305	305	4Ø25.5	36.9	444	1333	170
2	305	305	4Ø25.5	34.2	444	800	218
3	305	305	4Ø25.5	35.1	444	711	220
4	203	203	4Ø20.0	42.3	442	169	180
5	305	305	4Ø25.5	36.1	444	1067	208
6	305	305	4Ø25.5	34.8	444	1778	146
7	305	305	4Ø25.5	38.3	444	1333	187
8	305	305	4Ø25.5	43.6	444	1044	201
9	305	305	4Ø25.5	35.4	444	916	210
10	305	305	4Ø25.5	52.9	444	1178	227
11	305	305	4Ø25.5	49.5	444	1067	234
12	305	305	8Ø25.5	42.6	444	978	252
13	305	305	8Ø25.5	37.1	444	1333	225
14	406	406	8Ø25.5	38.8	444	2418	262
15	406	406	8Ø32.3	38.4	414	2795	285
16	406	406	8Ø32.3	46.2	414	2978	213
17	305	305	4Ø25.5	39.6	444	800	242
18	305	305	4Ø25.5	39.2	444	1000	220

* all columns have length (L) of 3.81 m long

Table 3. Details of Dotreppe et al. (1997)

No	b (mm)	h (mm)	steel bars (mm)	f'_c (MPa)	f_y (MPa)	P_{app} (kN)	t (min)

1*	300	300	4Ø16	33.9	576	950	61
2*	300	300	4Ø16	35.4	576	622	120
3*	300	300	4Ø16	29.3	576	422	116
4‡	300	300	4Ø16	29.3	576	1270	63
5‡	300	300	4Ø16	28.6	576	803	123
6‡	300	300	4Ø25	26.2	591	878	69
7‡	200	300	4Ø12	30.6	493	611	107
8‡	200	300	4Ø12	27.3	493	620	97

* $L = 3.9\ m$
‡ $L = 2.1\ m$

Table 4. Details of Hass (1986)

No	b (mm)	h (mm)	steel bars (mm)	f'_c (MPa)	f_y (MPa)	P_{app} (kN)	t (min)
1*	300	300	6Ø20	24.1	487	930	84
2*	300	300	6Ø20	24.1	487	930	138
3‡	300	300	6Ø20	34.1	487	880	108
4**	300	300	6Ø20	24.1	487	800	58
5*	200	200	4Ø20	24.1	487	420	58
6*	200	200	4Ø20	24.1	487	420	66
7‡	200	200	4Ø20	24.1	487	340	48

* $L = 3.76\ m$
‡ $L = 4.76\ m$
** $L = 5.76\ m$

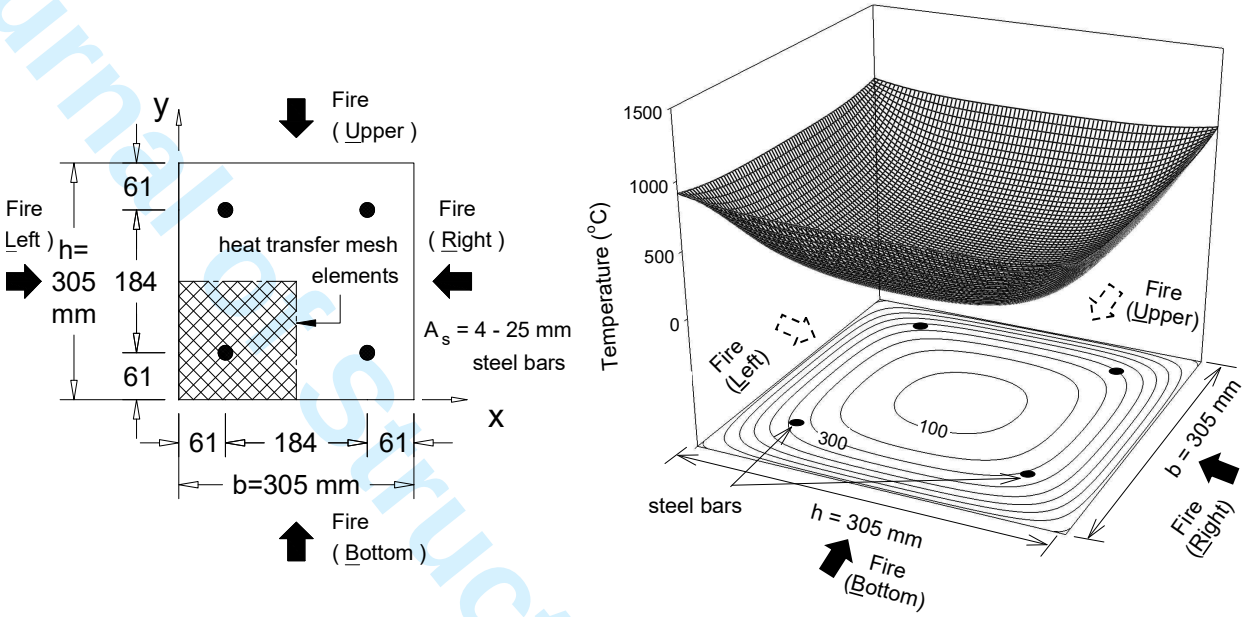

a) column section and mesh.

b) 1 hr ASTM-E119 temperature contour.

Fig. 1. Heat transfer analysis using FDM.

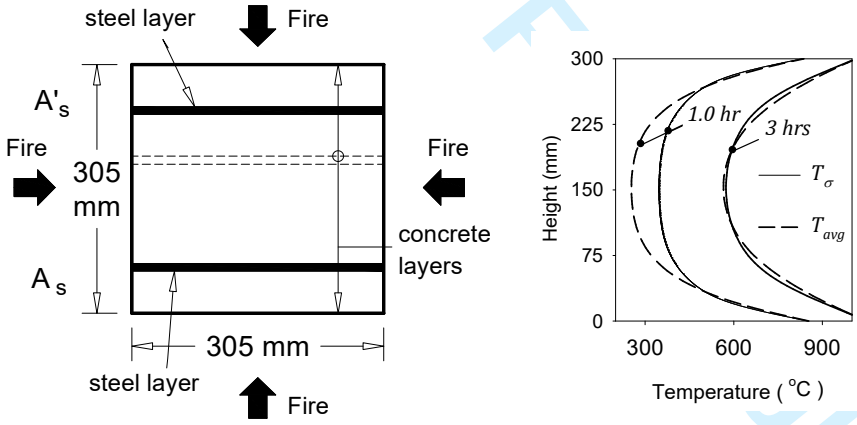

Fig. 2. Average temperature distribution.

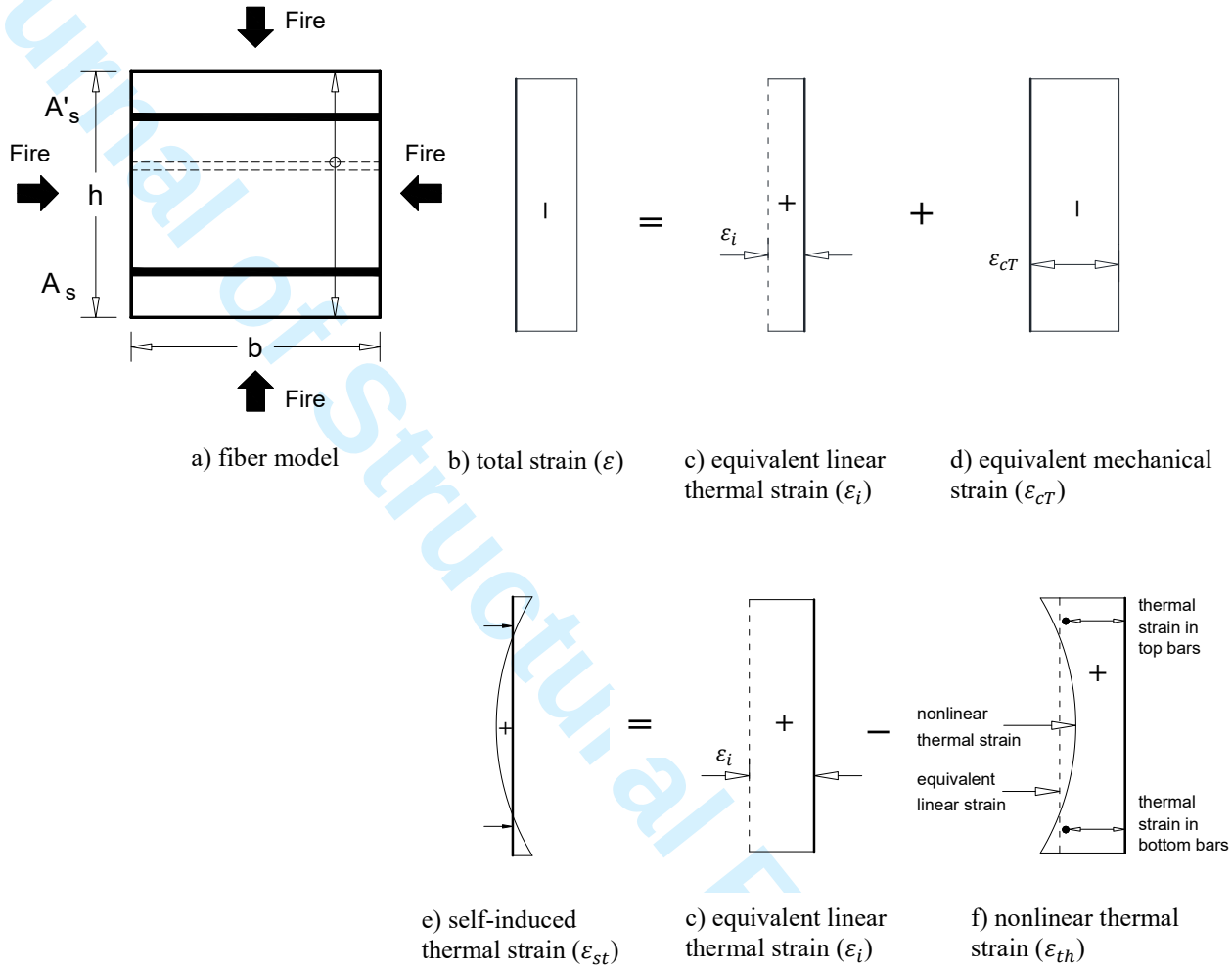

a) fiber model b) total strain (ε) c) equivalent linear thermal strain (ε_i) d) equivalent mechanical strain (ε_{cT})

e) self-induced thermal strain (ε_{st}) c) equivalent linear thermal strain (ε_i) f) nonlinear thermal strain (ε_{th})

Fig. 3. Sectional analysis approach for axially loaded RC sections exposed to fire.

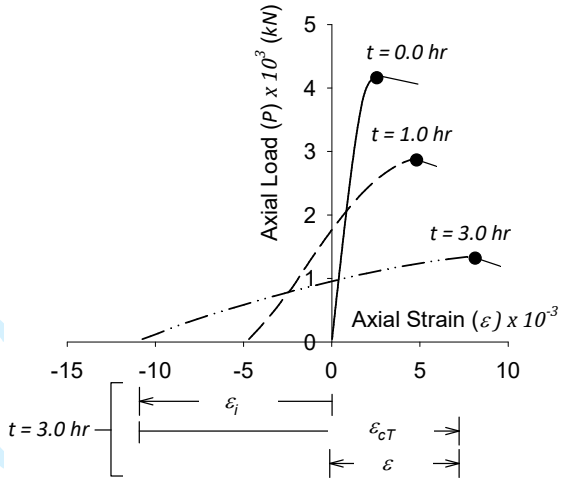

Fig. 4. P–ε relationships for a 305 mm square column at different fire durations.

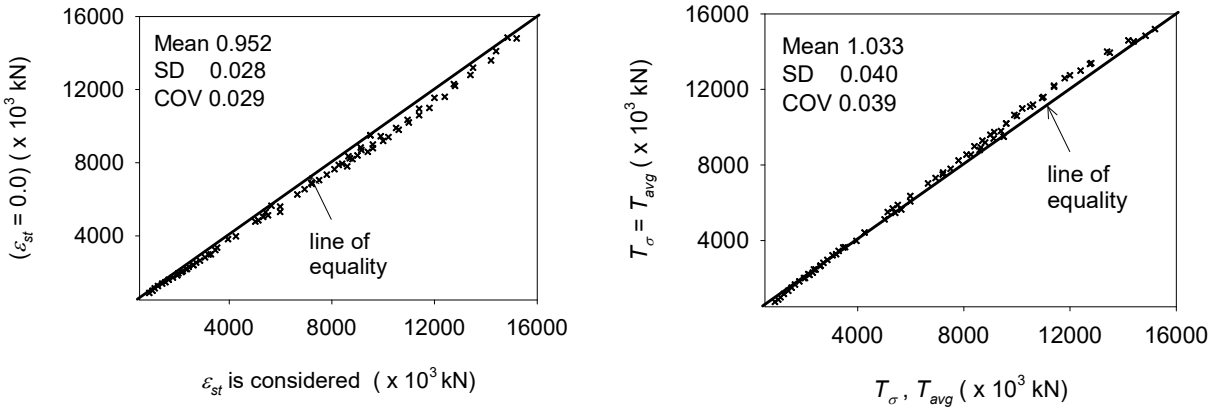

a) ε_{st} b) T_σ

Fig. 5. Effect of different parameters on sectional analysis results.

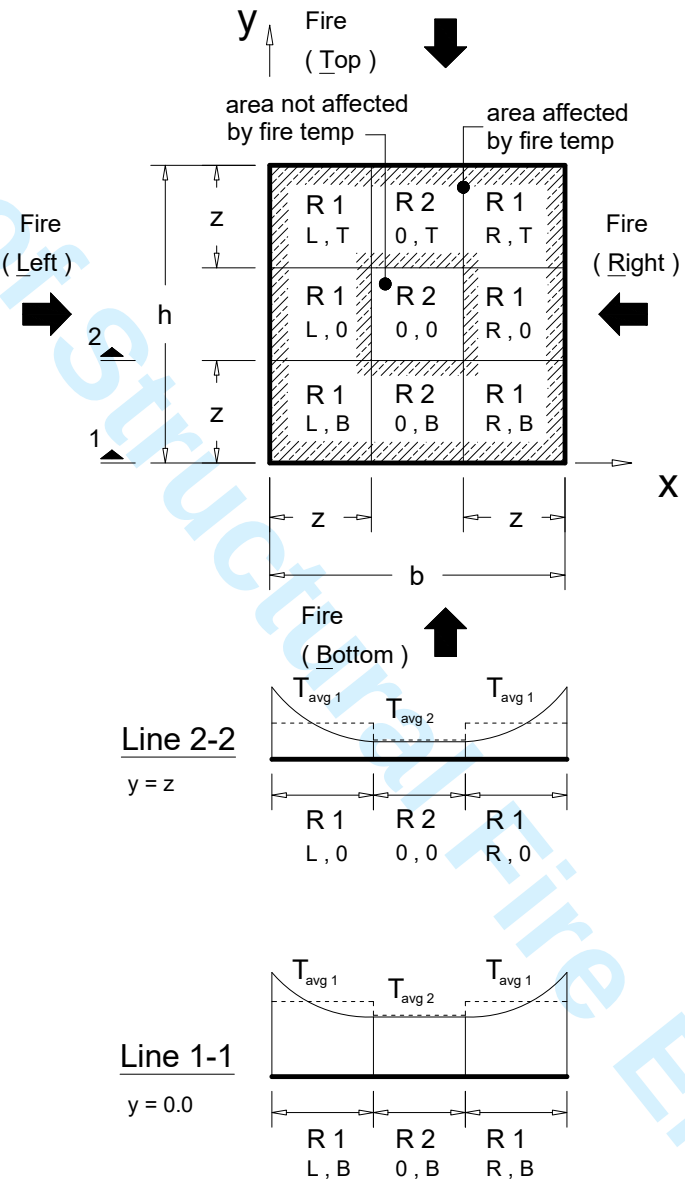

Fig. 6. Temperature calculation of example RC column ($z \leq b/2$).

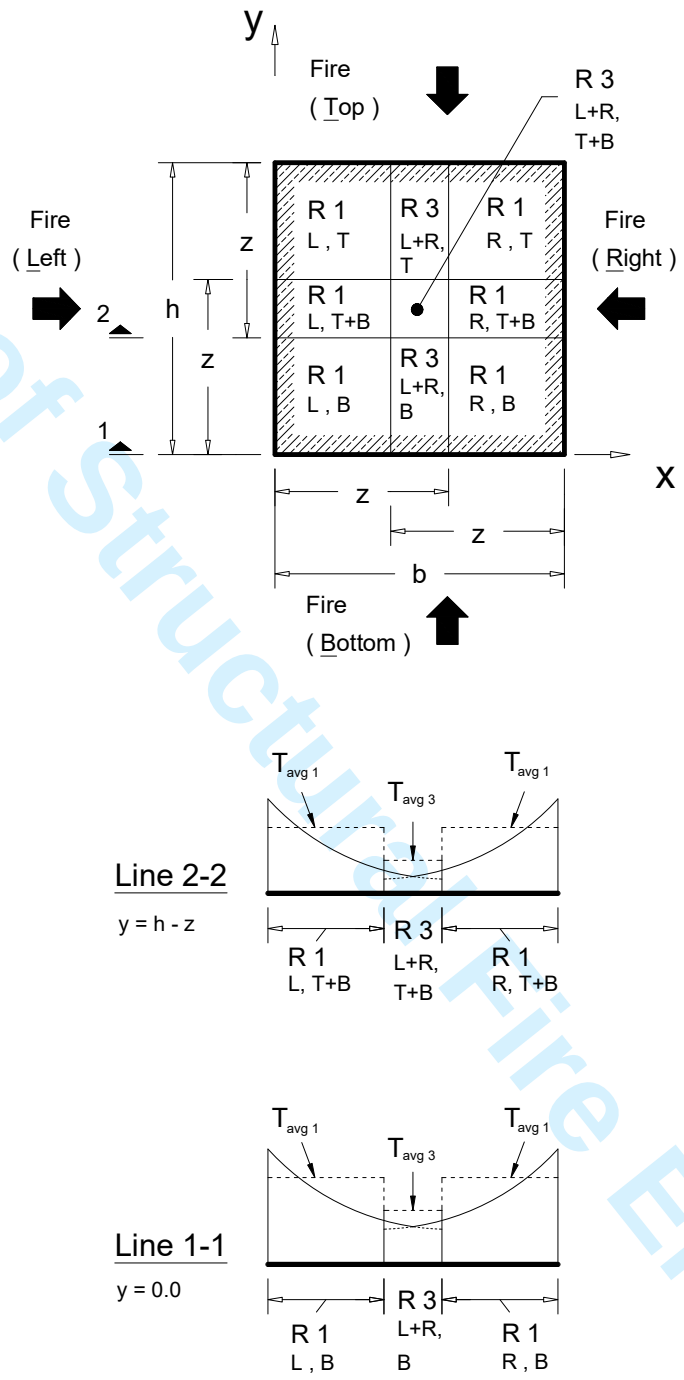

Fig. 7. Temperature calculation of example RC column ($z > b/2$).

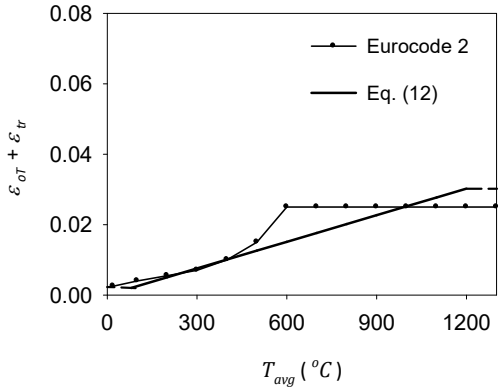

Fig. 8. Variation of $\varepsilon_{oT} + \varepsilon_{tr}$ at elevated temperatures.

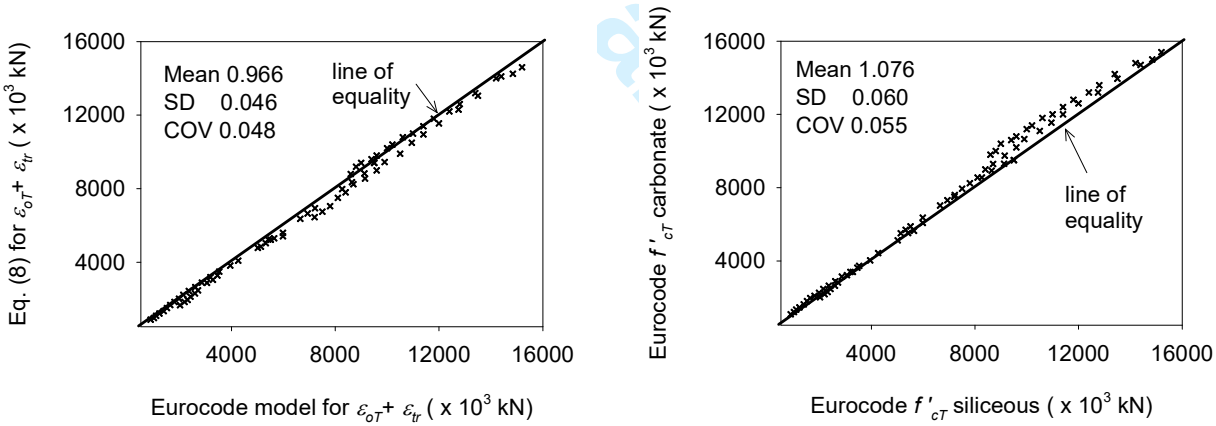

a) proposed Eq. (8) b) aggregate type

Fig. 9- Effect of different parameters on sectional analysis results.

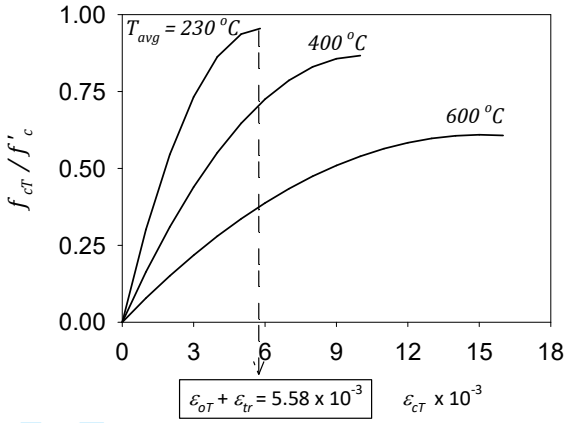

Fig. 10. Concrete stress-strain relationship at different T_{avg} values.

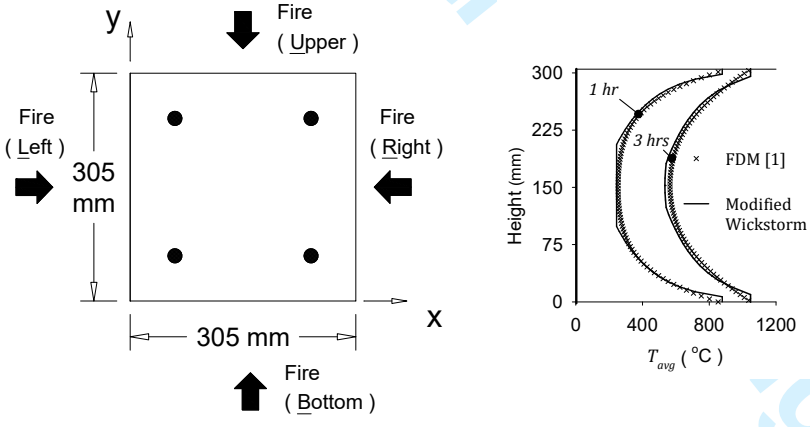

a) four-face heated RC section

b) T_{avg} dist

Fig. 11. T_{avg} distribution of the example RC column.

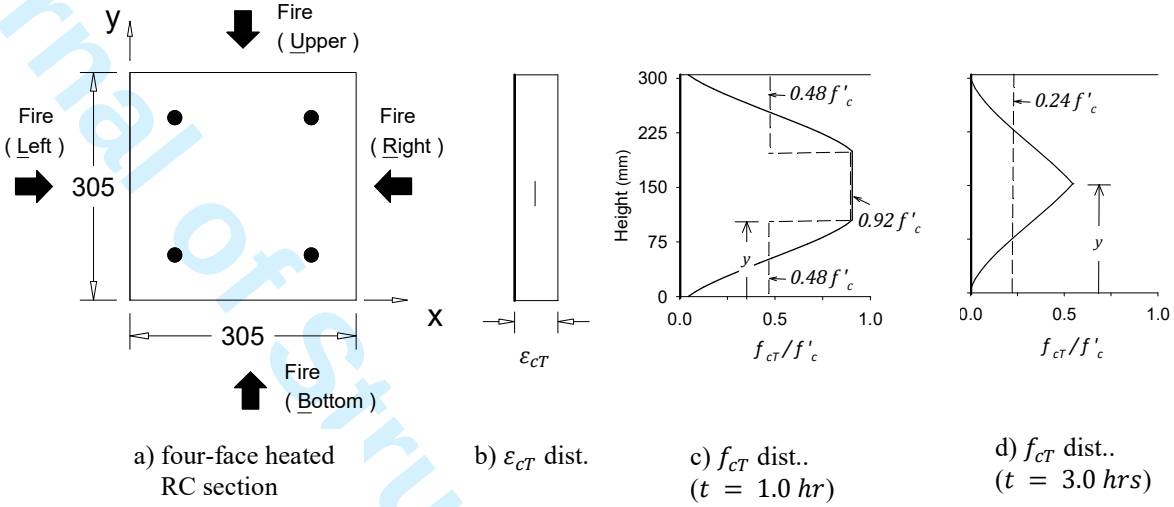

a) four-face heated RC section

b) ε_{cT} dist.

c) f_{cT} dist.. ($t = 1.0\ hr$)

d) f_{cT} dist.. ($t = 3.0\ hrs$)

Fig. 12. Average compression stresses distribution.

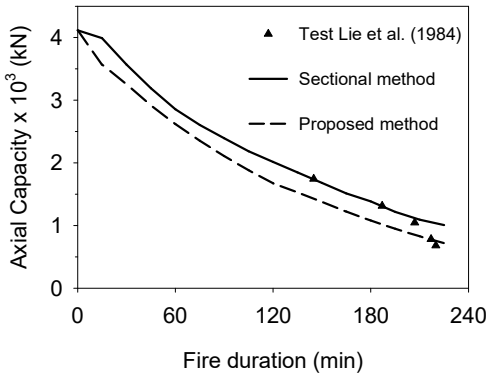

Fig. 13. Axial capacity predictions of example column.

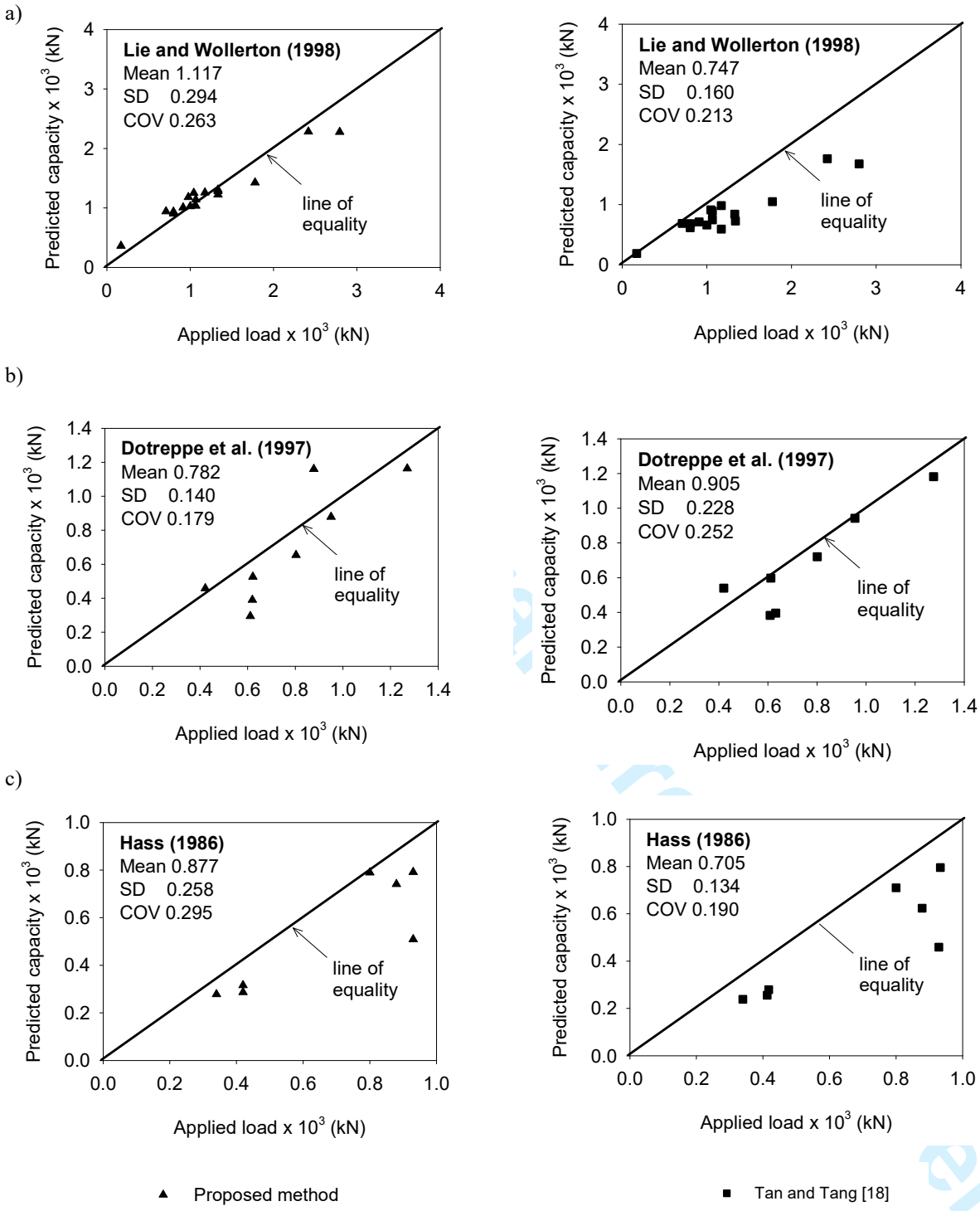

Fig. 14. Proposed method predictions for different experimental works.